# Quantized Hamilton dynamics describes quantum discrete breathers in a simple way

Kirill Igumenshchev* and Oleg Prezhdo†
*Department of Chemistry, University of Rochester, Rochester, New York 14627, USA*
(Received 29 March 2011; revised manuscript received 17 June 2011; published 29 August 2011)

We study the localization of energy in a nonlinear coupled system, exhibiting so-called breather modes, using quantized Hamilton dynamics (QHD). Already at the lowest order, which is only twice as complex as classical mechanics, this simple semiclassical method incorporates quantum-mechanical effects. The transition between the localized and delocalized regimes is instantaneous in classical mechanics, while it is gradual due to tunneling in both quantum mechanics and QHD. In contrast to classical mechanics, which predicts an abrupt appearance of breathers, quantum mechanics and QHD show an alternation of localized and delocalized behavior in the transient region. QHD includes zero-point energy that is reflected in a shifted energy asymptote for the localized states, providing another improvement on the classical perspective. By detailed analysis of the distribution and transfer of energy within classical mechanics, QHD, and quantum dynamics, we conclude that QHD is an efficient approach that accounts for moderate quantum effects and can be used to identify quantum breathers in large nonlinear systems.

DOI: 10.1103/PhysRevE.84.026616 PACS number(s): 46.40.−f, 03.65.Ge, 03.65.Sq, 03.65.Xp

## I. INTRODUCTION

A chain of coupled nonlinear sites often exhibits spontaneous localization of energy [1,2]. This phenomenon is known as discrete breathers, in this paper referred to as breathers. The localization occurs due to loss of resonance between the sites. As a result, the sites stop exchanging energy. Proven mathematically [2], [3]], this phenomenon can be found in a number of physical systems [4,5]. The existence of quantum breathers has been shown by quantization of classical solutions in both integrable [2] and nonintegrable systems [6]. Quantum breathers are essentially tunneling modes. In classical mechanics, the energy is localized. In quantum mechanics, the energy tunnels very slowly between lattice sites. Quantum breathers have been observed experimentally [5] in interacting Josephson junctions [7], Bose-Einstein condensates [8], crystals [9], quantum dots [10], molecules [11], and biological polymers [12]. Systems containing breathers are mostly nonintegrable, and, before the era of powerful computers, they were not accessible for theoretical analysis. These systems cannot be treated with standard linear methods and require a special theory that accounts for nonlinear effects.

The growth of nanoscale science and technology emphasizes the importance of quantum effects and requires the development of efficient approaches for modeling quantum dynamics. A fully quantum study of discrete breathers in a multidimensional system is extremely demanding computationally. Breathers are investigated classically with suitably parametrized models [13,14], or quantum mechanically using systems of drastically reduced dimensionality [15–18]. The first approach neglects quantum effects. The alternative scheme often employs truncated basis sets [19–21]. Quantized Hamilton dynamics (QHD) [22–27], quantal cumulant dynamics [28], correlated electron-ion dynamics [29], semiquantal theory [30], and related approaches offer a compromise, allowing one to include moderate quantum effects. Additional quantum information can be obtained at a cost that is only twice the expense of classical mechanical calculation [25]. One can even use a user-friendly QHD package for MATHEMATICA [31] to experiment with simple systems.

Recent applications of QHD to various quantum systems [24,25,32] showed that it is well suited to account for such quantum effects as zero-point energy, dephasing, interference, quantum correlations, and tunneling. The study of the Henon-Heiles problem [32] indicated that QHD can be applied successfully to multidimensional nonlinear systems. In this work, we extend the previous studies and apply QHD to a system in which the nonlinearity is more challenging and plays a critical role.

The system of two coupled pendula illustrates the breathers phenomenon (Fig. 1). If the initial amplitude of the first pendulum is small and the second pendulum starts at rest, the energy flows freely between the two pendula. As the initial amplitude of the first pendulum increases, the nonlinearity begins to dominate over the coupling, and an off-resonance condition develops. The energy does not transfer to the second oscillator and remains within the first oscillator for a very long time. This simple example explains the origin of classical discrete breathers. A formal introduction to discrete breathers in a two-site model for both classical and quantum mechanics can be found in Ref. [5]. This reference also discusses breathers arising in an infinite lattice.

Quantum breathers show similar signatures [33,34]. If the Hamiltonian is symmetric with respect to the site indices, then a stationary energy distribution is also symmetric. A quantum equivalent of a classical discrete breather is a tunneling mode. As $\hbar \to 0$, the tunneling time between the sites approaches $\infty$. At low energies, an initial wave function delocalizes over the sites. However, as the energy increases, the initial wave function localizes on sites and can transfer onto the other sites only by tunneling [35]. These localized states are quantum mechanical counterparts of classical breathers. Both classical and quantum breathers draw substantial interest [5,36].

Our study focuses on the lowest order QHD approach due to its remarkable simplicity. Many other methods have been

*kigumens@mail.rochester.edu
†oleg.prezhdo@rochester.edu

 

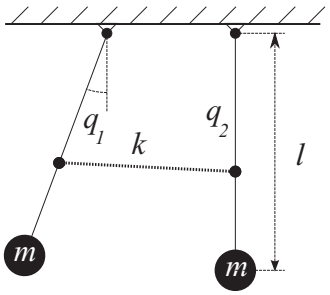


FIG. 1. Two pendula connected by a spring show signatures of breathers.

developed for studying quantum effects in large nonlinear systems and calculating semiclassical correlation functions and spectra. A representative, but by no means complete, list includes Heller's frozen Gaussians [37], the Herman-Kluk propagator [38,39] and its higher order extensions [39,40], coupled coherent states [41], matching-pursuit/split-operator Fourier transform [42,43], and coherent-state path integrals [44]. These approaches are based on averaging over multiple trajectories or finding roots for a boundary value problem. They can be more accurate than low order QHDs; however, they are more computationally demanding as well.

The current work combines research on quantum discrete breathers and semiclassical dynamics. Previous studies of quantum and classical discrete breathers in integrable and nonintegrable quartic dimers [2,5,6,35] have established the basis for understanding of the breather phenomena. The development and studies of semiclassical methods, and in particular QHD [25] and its application to modeling of tunneling in mildly nonlinear multidimensional systems [32], have revealed the benefits and limitations of the semiclassical methodology. This paper shows that a low order QHD can successfully account for the quantum effects seen with discrete breathers. The ability to model such quantum effects using a very simple and computationally efficient semiclassical technique presents a significant step toward narrowing the gap between complex, realistic systems and models of quantum breathers.

The paper is constructed in the following way. We introduce the investigated system, its Hamiltonian, and the initial conditions. The implementation of QHD and quantum dynamics are described after that. The results section contains two parts. The first part focuses on the advantages of QHD over classical dynamics. In particular, the system's dynamics and time-averaged energies are analyzed. The second part of the results section compares the classical and QHD results to quantum-mechanical calculations in the same potential. The paper concludes with a discussion and summary of the key results.

## II. METHODS

In this section, we define the system, its Hamiltonian, and the initial conditions for the classical dynamics and QHD. We also detail the numerical techniques used to propagate the classical and QHD trajectories and to solve the quantum-mechanical problem.

### A. Classical Hamiltonian and initial conditions

We focus on a simple system that exhibits signatures of breathers seen in realistic systems. At the same time, this system can be treated not only with classical mechanics and QHD, but also with quantum mechanics. The model is composed of two linearly coupled anharmonic oscillators. Figure 1 depicts its qualitative representation. The system Hamiltonian is

$$H = \frac{p_1^2 + p_2^2}{2} + c_h\left(q_1^2 + q_2^2\right) + c_a\left(q_1^4 + q_2^4\right) + c_c q_1 q_2. \quad (1)$$

Here, $c_h = 1/2$ defines the harmonic potential, while the constants $c_a$ and $c_c$ quantify the anharmonicity and the linear coupling strength, respectively. In the discussion below, all terms containing only the index for the first or the second site are used to define the corresponding site energy. The energy stored in the coupling part of the Hamiltonian is given by the last term containing coordinates of both sites.

Breathers can be identified by interruption of energy flow between the two oscillators, resulting in a long-lasting localization of energy with one of them. Such energy localization is the main signature of breathers. Here, it is analyzed by considering the dynamics of the energy transfer. The initial energy on the first oscillator is controlled by displacing the coordinate $q_1$. The second oscillator is at rest and, accordingly, the remaining variables, $q_2$, $p_1$, and $p_2$, are 0 at $t = 0$. All parameters are given in atomic units, $m = 1$ and $\hbar = 1$.

The anharmonicity and coupling parameters are $c_a = 0.005$ and $c_c = 0.1$; they control the *transient region* (TR). We define the TR as the region of energy that separates the regions dominated by local and normal modes. If the initial energy on the displaced site is lower than the energy of the transition region, then the energy fully transfers to the other site; if the initial energy is higher than the energy of the transition region, then it completely localizes on the initial site in classical mechanics and can only tunnel to the other site in quantum mechanics. Quantum mechanics allows the TR to contain both normal and local modes [35]; in contrast, in classical mechanics, the TR corresponds to a single value of energy referred to as the separatrix. We choose the parameters $c_a$ and $c_c$ such that the TR appears on the scale of the few quanta.

### B. Quantized Hamilton dynamics

Starting with the Heisenberg formulation of quantum mechanics, QHD obtains semiclassical approximations by truncating the hierarchy of Heisenberg equations of motion for quantum observables. At the second order of approximation for the momentum and position observables [25], QHD incorporates evolution of $\langle P^2\rangle$, $\langle \frac{PQ+QP}{2}\rangle$, and $\langle Q^2\rangle$ in addition to the classical-like $\langle P\rangle$ and $\langle Q\rangle$ variables. Classical mapping quantized Hamilton dynamics (CM-QHD) is an alternative representation of the second order QHD [25]. In CM-QHD, conservation of the Heisenberg uncertainty relationship is used to reduce the QHD for the second order $\langle P^2\rangle$, $\langle \frac{PQ+QP}{2}\rangle$, and $\langle Q^2\rangle$ variables to the Newtonian dynamics of the particle width $s$ and its conjugate momentum $p_s$. Such mapping further reduces the computational cost of QHD. The CM-QHD

Hamiltonian corresponding to the original Hamiltonian of our system, Eq. (1), is

$$H = \frac{p_1^2 + p_2^2 + p_{s1}^2 + p_{s2}^2}{2} + c_h\left(q_1^2 + q_2^2 + s_1^2 + s_2^2\right) + c_a\left(q_1^4 + q_2^4 + 6q_1^2 s_1^2 + 3s_1^4 + 6q_2^2 s_2^2 + 3s_2^4\right) + c_c q_1 q_2 + \frac{1}{8s_1^2} + \frac{1}{8s_2^2}. \quad (2)$$

Here, $q$ and $p$ are the classical-like position and momentum variables, and $s$ and $p_s$ are the quantum-mechanical width and its conjugate momentum. Just as in the classical mechanical Hamiltonian, Eq. (1), all terms containing only the index for the first or the second site define the QHD energy of the corresponding site, while the term containing both indices gives the energy stored in the coupling. The initial conditions of the additional variables are set to $s_i = 1$ and $p_{si} = 0$, for $i = 1,2$, corresponding to the ground state of the harmonic oscillator.

The evolution of the QHD variables is obtained using classical Hamilton equations of motion for the above Hamiltonian, Eq. (2). This system of nonlinear coupled differential equations is not integrable and requires a numerical approach. Our C++ code uses the eighth order adaptive step-size Runge-Kutta library from Numerical Recipes 3, section 17.2.4 [45]. For the given parameters of the Hamiltonian and the step of 0.1 time units, the integration performs well for $t < 2000$ time units. This is sufficient for our purpose. The integration tends to break down at long times, especially in the transient region. This limitation brings noise to some of the plots.

### C. Quantum mechanics

QHD generates dynamics that can be viewed as a classical trajectory with an addition of a quantum correction. We would like to compare the QHD calculation of energy localization to a quantum equivalent. Similarly to classical dynamics, QHD equations of motion produce a trajectory in the $(p,q,p_s,s)$ space. Averaging the energy of each oscillator over the trajectory gives a quasistationary energy distribution. Its quantum equivalent is the energy distribution within a stationary state. Presenting these stationary states in a basis that is a direct product of the basis sets for each oscillator allows us to characterize the desired energy localization.

Equation (3) is a quantum-mechanical equivalent of the classical and QHD Hamiltonians, Eqs. (1) and (2), respectively:

$$\begin{aligned} H &= c_h H_h + c_a H_a + c_c H_c, \\ H_h &= a^\dagger a + a a^\dagger, \\ H_a &= \frac{1}{16}(aaaa + aaaa^\dagger + \cdots + a^\dagger a^\dagger a^\dagger a^\dagger), \\ H_c &= \frac{1}{4}\sum_i (a_i a_{i+1} + a_i a_{i+1}^\dagger + a_i^\dagger a_{i+1} + a_i^\dagger a_{i+1}^\dagger). \end{aligned} \quad (3)$$

The basis states $|N_1 N_2\rangle$ are direct products of the eigenstates of the one-dimensional number operators for each oscillator.

The eigenvalue problem for the above Hamiltonian is solved using a C++ code with the linear algebra operations implemented in the GMM++ library. The eigenstates considered below are limited to quantum numbers of 25 or less. The basis set involving 35 states for each oscillator was sufficient to obtain converged results.

## III. RESULTS

The semiclassical QHD method fits between classical and quantum formalisms. The computational expense of the second order QHD used here is very similar to that of classical mechanics. Our goal is to compare the QHD results with the classical and quantum data and to establish whether this very simple semiclassical theory can capture qualitatively and perhaps quantitatively the quantum signatures of breathers. The next section shows how QHD is an improvement on classical dynamics. We study in detail the evolution of the coordinate and average energy of each oscillator. The second section compares the average energy distributions in QHD and quantum mechanics.

### A. QHD advantages over classical dynamics

The dynamics of the nonlinear system described by the Hamiltonian of Eq. (1) depends on the relative magnitudes of the anharmonic and coupling terms. These magnitudes can be controlled either by the values of the constants $c_a$ and $c_c$ or by the initial conditions, and in particular by the displacement of the coordinate of the first oscillator $q_1$. When either the nonlinearity or the coupling significantly dominates, QHD and quantum and classical dynamics all behave in a similar way. If the nonlinearity is much smaller than the coupling, the dynamics is well described by normal modes (defined below). In the opposite case, the dynamics become localized on one or the other oscillator. Figure 2 demonstrates this behavior. The figure shows QHD of position coordinates for the two oscillators: $q_1$ [solid (red) line] and $q_2$ [dashed (green) line]. Aside from a zero-point energy correction, the classical plots would look exactly the same [1–3]. The two plots in Fig. 2 differ in the initial amount of energy on site 1. For the bottom plot, $q_1 = 0.1$. Throughout the dynamics, the amplitude of the oscillations on site 1 periodically approaches 0, while at the same time, the amplitude on site 2 approaches the initial displacement of the first oscillator. Periodically, the energy of site 1 fully transfers to site 2 and back. There is no localization, and both position variables oscillate with the same amplitude. This is an example of an approximately linear behavior that can be described with normal modes.

In order to proceed with the subsequent discussion, a workable definition of the local and normal mode dynamical regimes is needed. One can consider two limits. The first is the linear limit ($c_a \ll c_c$), where the dynamics can be described using normal modes, the sites are invariant under permutation, and there is a rapid, full transfer of energy between the sites. In the opposite, nonlinear limit ($c_c \ll c_a$), the anharmonicity is strong, the sites are essentially decoupled and not invariant under permutation, and slow energy transfer occurs through tunneling. The two limits are separated by the transient region that exhibits both types of behavior. The system is considered to be in the *normal mode* region if the energy averaged over a sufficiently long time converges to the same value for all sites. If the energy converges to a much higher value on one

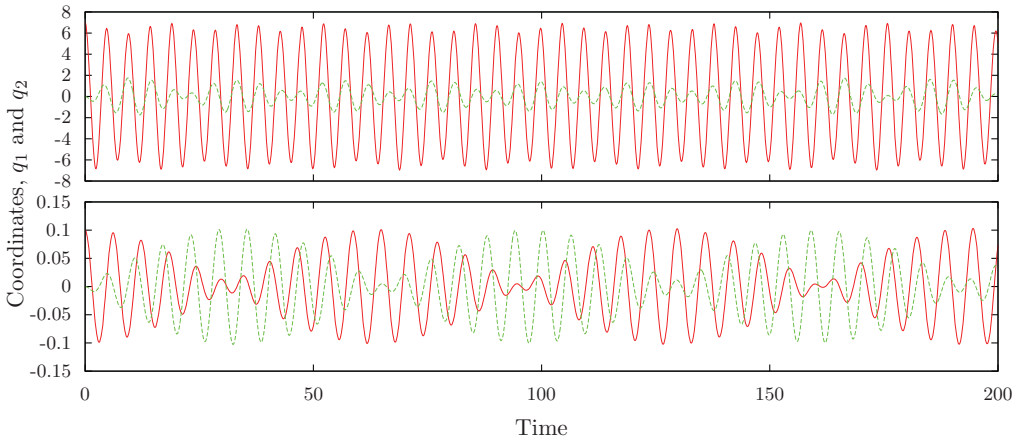


FIG. 2. (Color online) Classical-mapping QHD trajectories of the position coordinates of the two oscillators $q_1(t)$ [solid (red) line] and $q_2(t)$ [dotted (green) line] for different initial conditions: (top) $q_1(0) = 7.0$ and (bottom) $q_1(0) = 0.1$. In all cases, $q_2(0) = 0$. The top and bottom panels show the localized and delocalized regimes.

site than on the other site, then the system is regarded to be in the *local mode* region. If the dynamics switches from one behavior to the other, e.g., local dynamics is followed by rapid energy transfer, which in turn is followed by another period of local dynamics, then the system is in the transient region. At present, the classification is based on the $t = 2000$ simulation time, due to numerical limitations. This time scale is much larger than the energy transfer time in the linear limit. In classical mechanics, the time scale of the energy transfer in close proximity of separatrices approaches infinity, but this effect is dominated by an abundance of chaotic behavior. The effectiveness of the above definition is illustrated below by comparison of QHD to classical and quantum dynamics.

By changing the initial energy on site 1, we can control whether the nonlinearity dominates the coupling. The higher order terms in Eq. (1) grow faster than the harmonic terms. Therefore, at higher displacements, the nonlinear terms contribute more to the energy than the harmonic terms or the linear coupling, and the system becomes dominantly anharmonic.

The top panel of Fig. 2 is an example of breather modes. The initial displacement on site 1 is high ($q_1 = 7.0$), and the nonlinear effects dominate the linear coupling, Eq. (1). The energy of site 1 does not fully transfer to site 2. The amplitude of the position on site 1 periodically decreases but always remains high. This is an example of a spatially localized motion that is periodic in time. Quantum-mechanically, the energy can tunnel between the two modes. However, the quantum tunneling time is very long, and quantum effects are insignificant on the time scale of the simulation.

Both classical and quantum dynamics transition from normal to local modes as the energy increases. In classical dynamics, the transition is sharp and corresponds to a separatrix in the phase space. If the energy is above the separatrix, the energy does not flow from one site to the other. In quantum dynamics, there is a transient region containing alternating local and normal modes [35]. Because QHD accounts for quantum effects, it exhibits signatures of both quantum and classical dynamics. One may expect that QHD differs most from classical dynamics in the transient region.

The QHD approach, even at its lowest order, offers a significant qualitative improvement over classical dynamics. The transition from the normal to the local mode regime is gradual in QHD. Similarly to quantum mechanics, which contains alternating local and normal mode eigenstates, QHD trajectories jump between normal and local regimes in the transient region. This behavior is illustrated in Figs. 3 and 4. In the top panel of Fig. 3, the energy starts in a local mode ($t < 350$) and then goes into a normal mode ($t > 350$). The bottom panel shows the opposite scenario: the system starts in a normal mode ($t < 300$) and goes into a local mode ($t > 300$). Such switching between the normal and local regimes is not possible within a single classical trajectory. In classical mechanics, the magnitude of the initial energy uniquely defines the dynamic regime.

On the short time scale, quantum wave packets exhibit classical-like behavior. This fact is reflected in QHD. QHD trajectories with $q_1(0) < 5.2$ start in the normal mode regime, while trajectories with $q_1(0) > 5.2$ are initially in the local regime. The classical separatrix for the same Hamiltonian, Eq. (1), corresponds to $q_1 \approx 5.2$. Quantum behavior becomes apparent at longer times. Running QHD trajectories for $t > 500$ is sufficient to see quantum effects (Fig. 3).

Longer time QHD allows us to observe a more complex behavior. In Fig. 4, the system goes from the local to the normal mode regime and back to the local regime. Even more interestingly, the energy can start localized on one oscillator and transfer to the local mode on the other oscillator (see the bottom panel of Fig. 4). This process is akin to quantum-mechanical tunneling. Within QHD, tunneling occurs by a classical-like dynamics in the width variable [25]. In the current simulation, the transfer of energy between the two local modes proceeds by a temporary energy flow into and out of the width coordinates. At times $400 < t < 1000$ in the top panel of Fig. 4 and $700 < t < 1300$ in the bottom panel, significant amounts of energy are stored in the width variables. In the first case, the energy comes back from the width variables to $q_1$, while in the second case it transfers to $q_2$. The study of the influence of classical chaos on quantum-mechanical tunneling is relevant in the present case [6]. Applying this connection

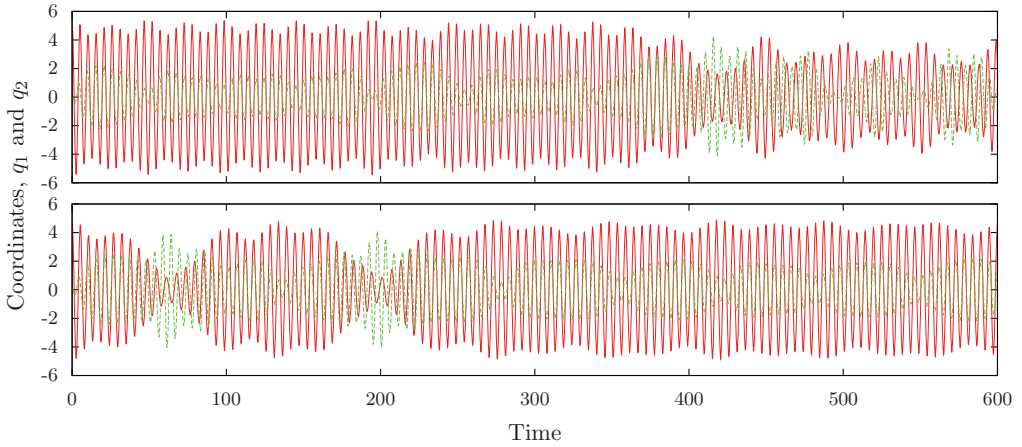


FIG. 3. (Color online) Same as Fig. 2 but for different initial conditions for the $q_1$ variable: (top) $q_1(0) = 5.5$ and (bottom) $q_1(0) = 4.893$. These plots show signatures of both local and normal modes within a single QHD trajectory. The trajectory in the top panel starts in a local mode and then switches to a normal mode. The trajectory in the bottom panel does the opposite. In contrast, a classical trajectory would be in either the local or the normal mode regime at all times.

between quantum and classical mechanics to QHD can be used to rationalize how QHD handles tunneling.

Further analysis of the energy localization and flow can be achieved by considering time-averaged properties. In particular, it is important to systematically investigate the transfer of energy as a function of the initial amount of energy on site 1. Figure 5 shows the relationship between the average energies of the first and second sites, $\langle H_1(q_1)\rangle$ and $\langle H_2(q_2)\rangle$, plotted along the $x$ and $y$ axes, respectively. Each point corresponds to a different initial displacement of the position of oscillator 1. Starting from 0, the initial displacement was incremented by 0.001. Both QHD and classical dynamics were run for 2000 time units, and the energy contained in each mode was averaged over these trajectories. The energy terms $\langle H_2(q_2)\rangle$ vs. $\langle H_1(q_1)\rangle$ shown in Fig. 5 exclude the linear coupling, Eq. (1). The energy stored in the coupling is much smaller than the energy of the sites. First, we discuss the familiar result of classical dynamics. Then, we consider the differences offered by QHD.

The modulation of the normal mode dynamics seen in QHD compared to the classical dynamics arises due to the fact that the classical-like position variables are coupled to the width variables in the second order QHD. The QHD extension of the classical phase space introduces additional frequencies to the dynamics.

The classical data shown by the green (light gray in black-and-white) symbols in Fig. 5 increase linearly up to the separatrix point around (8,8), then jump discontinuously to (10,6) and asymptotically approach the $x$ axis. Before the separatrix, the system is in the normal mode regime. The energy is equally distributed between two sites, even though initially there was energy only on one of the sites. While the nonlinearity always grows faster than the coupling, below the separatrix, the interplay between the nonlinearity and coupling does not affect the amount of energy transferred. The energy is distributed evenly.

Above the separatrix, the energy suddenly localizes. After the point (8,8) the data jump to (10,6). Now the nonlinear

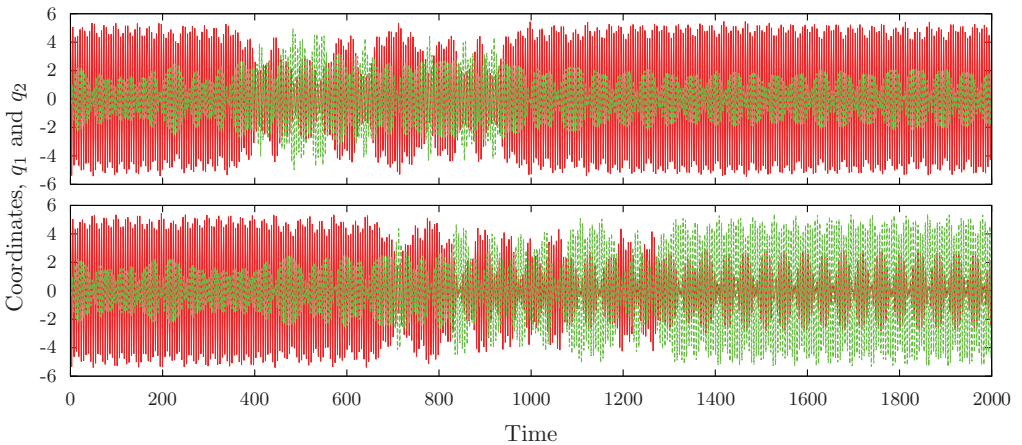


FIG. 4. (Color online) Same as Fig. 2 but for different initial conditions: (top) $q_1(0) = 5.504$ and (bottom) $q_1(0) = 5.476$. In both plots, the trajectory starts in a local mode, transitions into a normal mode, and then comes back into a local mode. In the top panel, the energy returns to the same oscillator where it started. In the bottom panel, the energy transfers from the first oscillator onto the second one.

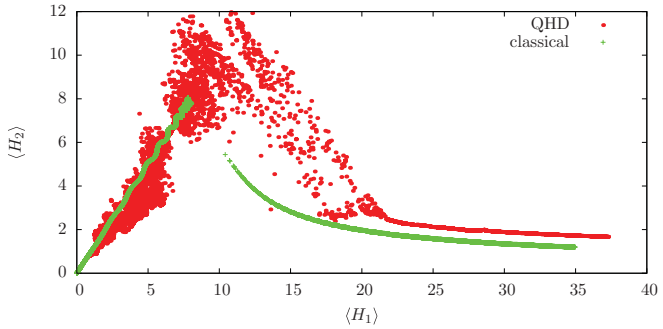


FIG. 5. (Color online) Distribution of energy between the two oscillators depending on the initial amount of energy in the first oscillator. Each point shows the time-averaged energy of the first and second oscillator, $\langle H_1 \rangle$ and $\langle H_2 \rangle$, respectively. The total energy is distributed equally between the oscillators at low energies and localized within the first oscillator at high energies.

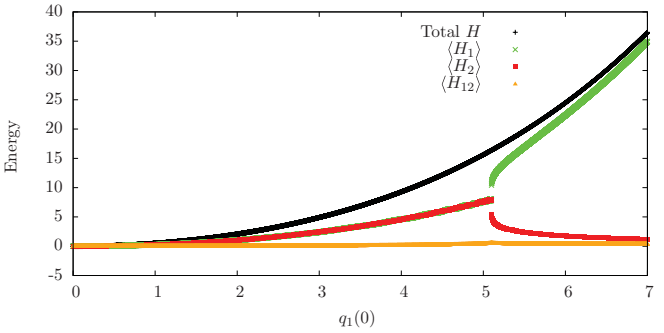


FIG. 6. (Color online) Total energy $H$ (black), energies of the first and second oscillators, $\langle H_1 \rangle$ (green) and $\langle H_2 \rangle$ (red), and interaction energy, $\langle H_{12} \rangle$ (orange), as functions of the initial displacement of the first oscillator, $q_1$. At $t = 0$, the second oscillator is at rest, $q_2 = 0$. The results are obtained using classical mechanics. In black-and-white, the green, red, and orange colors translate into light gray, dark gray and gray.

effects dominate over the coupling and drive the system off resonance. The energy deposited into one site does not transfer to the other site completely. Part of the energy still transfers, but as initial energy increases and the dynamics becomes more anharmonic, the amount of the transferred energy decreases.

The QHD data [red (dark gray in black-and-white) symbols in Fig. 5] show the same general trends as the classical results. However, there are a number of important qualitative and quantitative differences. Just as in classical mechanics, the QHD energy is delocalized between the sites at low energy. After the transient region, the energy localizes. Toward higher energies, the energy localizes even further. At the same time, QHD shows quantum effects, in particular, zero-point energy and tunneling. Zero-point energy shifts the QHD data to higher energies. The $\langle H_1(q_1) \rangle$ and $\langle H_2(q_2) \rangle$ values start above zero, and the asymptotic QHD curve is above the classical curve. Even more importantly for quantum breathers, the transition from the delocalized to the localized regime is much less abrupt in QHD than in classical mechanics. This provides a clear signature of quantum-mechanical tunneling.

The transient region of QHD is extended in energy. For some initial conditions within the transient region, the QHD energy is shared between the sites, while for other initial conditions it is localized. This alternation of the delocalized and localized behavior corresponds directly to the alternation of the localized and delocalized quantum-mechanical wave functions presented in the next section. Both tunneling and zero-point energy are responsible for extending the maximum of the transient region from (8,8) in classical mechanics to (11,11) in QHD.

Figures 6 and 7 illustrate the classical and QHD dependence of the time-averaged energies on the initial displacement of $q_1$. In addition to the time-averaged energies stored in each mode $\langle H_1 \rangle$ and $\langle H_2 \rangle$, the time-averaged interaction energy $\langle H_{12} \rangle$ and the total energy $H$ of the system are shown as well. These plots are similar to Fig. 5. The energies on the $y$ axis depend on the initial energy deposited on site 1. Since all coordinates besides $q_1$ and the QHD widths $s_1 = s_2 = 1.0$ are 0, $q_1$ controls the initial energy on site 1. Compared to classical dynamics, QHD shifts the energy by zero-point contribution and extends the transient region due to tunneling. Figures 6 and 7 indicate that the coupling energy is very small and that the total energy is conserved.

### B. Comparison of QHD to quantum mechanics

The quantum equivalent of classical breathers are tunneling states. High energy excitations present in the tunneling states are localized on individual sites. In contrast, at low energies, excitations are delocalized between the sites. The excess energy present in a quantum breather state can tunnel from one site to the other. Classical dynamics cannot describe tunneling or zero-point energy, while QHD can. This section compares the classical and QHD results to quantum mechanics. The focus is on energy distribution. First, we discuss how to visualize the quantum breather eigenstates. Then, we show how the quantum breather states correspond to the classical breathers, and we compare classical and QHD breathers to the quantum results.

A quantum-mechanical equivalent of Fig. 5, which presents the distribution of the time-averaged energy between the sites, is a figure showing the distribution of energy between the sites within stationary states. These data are presented as contour plots, with the $x$ axis corresponding to the energy on site 1 and the $y$ axis to the energy on site 2. Figure 8 illustrates how to read the contour plots. The quantum-mechanical calculations are performed in the basis that is a direct product of harmonic oscillator states $|N_1, N_2\rangle$. The quantum numbers $N_1$ and $N_2$

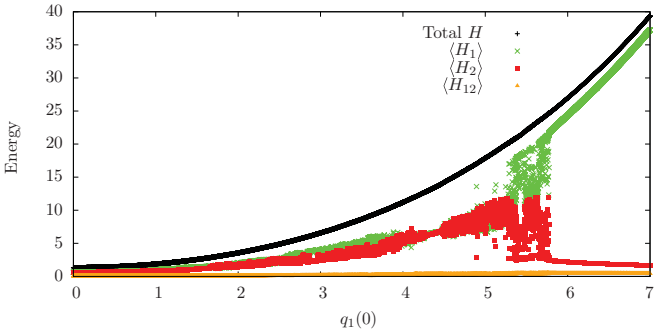


FIG. 7. (Color online) Same as Fig. 6, but for QHD.

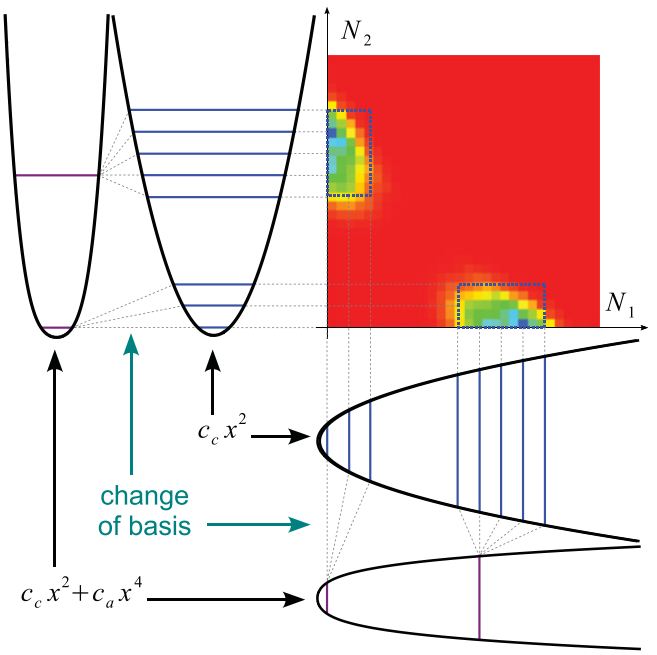


FIG. 8. (Color online) Rationalization of the contour plot showing a breather state. This localized eigenstate of the full two-dimensional Hamiltonian, Eq. (3), is formed from the eigenstates of the one-dimensional quartic Hamiltonians for each oscillator. The one-dimensional eigenstates mix, because the full Hamiltonian contains linear coupling. In turn, each eigenstate of the quartic Hamiltonian is expanded in the corresponding harmonic basis. The axes represent the quantum numbers of the harmonic basis. The figure shows that a tunneling (localized) state has density near the axes. The blue and yellow colors (dark and light gray in black-and-white) depict negative and positive parts of the wave function. Delocalized states, shown in Fig. 9, have density on the increasing diagonal.

are plotted along the $x$ and $y$ axes, respectively. An $(N_i, N_j)$ point on the plane describes the contribution of the $|N_i, N_j\rangle$ basis state to the eigenstate of the full Hamiltonian, Eq. (3).

The eigenstate shown in Fig. 8 is a tunneling state. Its density is located predominantly near the axes. Points localized near the $x$ axis correspond to eigenstates, in which the excitation is primarily on site 1. Similarly, points near the $y$ axis describe excitations localized on site 2. The tunneling state shown in Fig. 8 carries no density on the diagonal, indicating that harmonic oscillator levels that share energy between the sites do not contribute to this eigenstate.

The density of the state shown in Fig. 8 extends along the $N_1$ and $N_2$ axes. This is because this eigenstate of the full Hamiltonian, Eq. (3), involves a superposition of several harmonic states. At low energies, the quartic term is small, and eigenstates correspond closely to harmonic states. The linear coupling between the two oscillators creates states that are delocalized along the decreasing diagonal of the contour plot. The progression of states shown in Fig. 9 illustrates how states extended across the plane become localized near the axes.

Figure 9 is a quantum-mechanical counterpart of Fig. 5, obtained from classical mechanics and QHD. Both figures characterize the energy distribution between the two sites. In the quantum case, the system is discrete. The eight eigenstates of increasing energy shown in Fig. 9 illustrate how passing through the transient region influences the distribution of energy between the two oscillators in quantum mechanics. The first eigenstate is an example of a delocalized state. The energy is distributed evenly between the oscillators, and the contribution of the $N_1 = N_2$ harmonic basis states near the diagonal is large. The last plot is an example of a localized (tunneling) state. Just as in Fig. 8, it is located close to the axes and notably extended along the axes.

Consider the quantum behavior near the separatrix and compare it to classical mechanics and QHD, Fig. 5. In the classical case, the energy is shared between the sites until the separatrix point is reached at approximately 8 energy units in each site, with the total energy of about 16. Above the separatrix point, classical mechanics predicts sharp energy localization. The classical curve in Fig. 5 jumps abruptly from point (8,8) to point (10,6), with the same total energy.

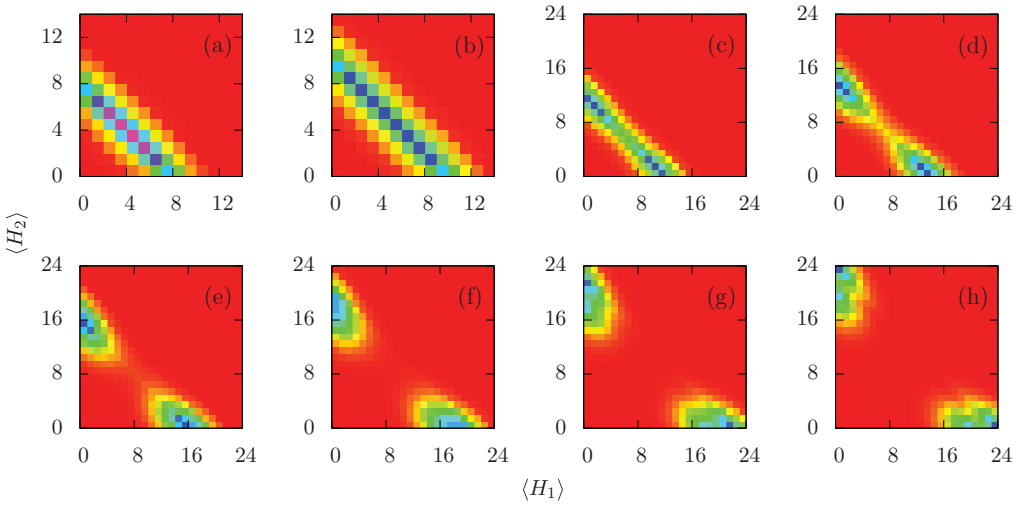


FIG. 9. (Color online) Eigenstates of the Hamiltonian, Eq. (1), at low and high energies. Figure 8 explains the notation. From (a) to (h), one observes a transition from delocalized to localized states. As the quantum numbers increase, the energy tends to localize within one or the other oscillator.

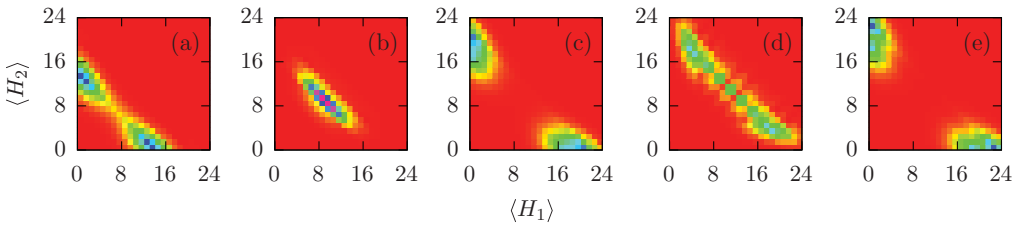


FIG. 10. (Color online) Same as Fig. 9, but for the energy of the transient region. One observes alternation between breather and delocalized states. A similar behavior is seen with QHD in Figs. 5 and 7.

The quantum state corresponding to the classical separatrix is shown in Fig. 9(e). In contrast to the classical behavior, the quantum state at this energy is already notably localized. Even the state at a much lower energy of about 12 [Fig. 9(d)] shows localization. In general, the transition from the delocalized to the localized regime is much smoother in quantum than in classical mechanics. QHD reflects this behavior. At the classical separatrix point (8,8) in Fig. 5, QHD shows a spread of points with various degrees of localization. Some delocalization is seen with QHD at lower energies as well. The transition from the delocalized to the localized behavior is much smoother in QHD than in classical mechanics. The qualitative change in the QHD behavior from the predominantly delocalized to the predominantly localized states is observed near the (11,11) point, corresponding to the quantum-mechanical Fig. 9(g), which shows a well-localized tunneling state.

In addition to describing a gradual transition from the delocalized to the localized regime, QHD reproduces another quantum effect: occurrence of both local and normal modes in the transient region. Figure 10 shows a quantum calculation for this phenomenon. Figure 10(a) has the same energy as the first local mode recognized by QHD at $q_1(0) = 4.9$ in Fig. 7. There are a number of local and normal modes in the transient region. Figures 10(b) and 10(c) are just two examples. Figure 10(d) is the last appearance of the normal mode recognized by QHD; it appears at $q_1(0) = 5.8$. In contrast to Fig. 10(a), Fig. 10(e) shows that, after the transient region, we have a dominant localization. In classical mechanics, the alternation between the local and normal modes does not exist (Figs. 5 and 6). Below the separatrix point, classical dynamics is delocalized, while above it classical mechanics predicts breathers. In contrast, QHD shows both types of behavior in the transient region. This is evident in the scatter of the data in Fig. 5 and the additional transition to and from the localized regime around $q_1(0) = 5$ in Fig. 7. We expect that higher order QHD [32] is able to model this phenomenon at a more quantitative level.

## IV. CONCLUDING REMARKS

This paper shows that QHD offers advantages over conventional classical and quantum mechanics for the description of quantum breathers in large systems. With an extremely small increase in the computational cost, QHD adds quantum effects to a classical trajectory. In particular, at the second order, which is only twice the cost of classical mechanics, QHD preserves zero-point energy and includes tunneling. Zero-point energy is reflected in the shift of the asymptote for the breather state energy, relative to the classical asymptote. Tunneling results in a gradual transition from the delocalized to the localized regime. The transition is abrupt in classical mechanics, while it is smooth in both quantum mechanics and QHD. Furthermore, the second order QHD qualitatively reproduces the alternation of the localized and delocalized behavior predicted by quantum mechanics in the transient region.

The current work used the second order QHD in the classical mapping formulation [25]. Each classical degree of freedom is "dressed" with a width variable, making this approach similar, but not fully identical, to the "thawed" Gaussian technique [46]. Classical mapping is particularly important for simulation of large systems. It allows one to use standard classical-mechanical tools in order to analyze the QHD dynamics, for instance, in the cases of numerical instabilities. The second order QHD formulated using an effective classical potential, Eq. (2), can be implemented within standard classical molecular dynamics codes. At the same time, the version of the second order QHD that can be mapped onto an effective classical Hamiltonian is a very low order approximation to quantum dynamics. It decomposes cross terms between different degrees of freedom to the first classical-mechanical order and therefore excludes quantum-mechanical correlations between different modes. Higher order QHD offer more quantum information and a better description of tunneling. In application to breathers, higher order QHD should improve the description of the transient region, making it smoother and creating a better picture of alternating normal and local modes.

Both classical dynamics and QHD are nonlinear approaches in a finite-dimensional phase space. This is in contrast to quantum mechanics, which is a linear theory in an infinite-dimensional Hilbert space. Numerical integration of the coupled nonlinear differential equations of classical mechanics and QHD becomes difficult in the transient region. One can notice noisy behavior of the results in this region in Figs. 6 and 7. Increasing the numerical accuracy of the classical and QHD calculations in the transient region would improve the quality of the results. The improvement can be achieved by using higher precision floating point operations or a higher order numerical integration technique.

Application of QHD to real systems may require the use of other potentials. For instance, the Morse potential may be needed in order to represent molecular vibrations. A generic potential can be expanded in a Taylor series, reducing the problem to a harmonic potential with higher order corrections [32]. Alternatively, one can develop QHD approximations using the raising and lowering operators for the Morse potential [24], or represent an arbitrary potential by combining more convenient potentials [47].

In order to bridge the gap between theory and experiment, one needs to consider the contribution of discrete breathers to the dynamics in thermal equilibrium [33,48,49]. For instance, QHD can be used to include moderate quantum effects in the relaxation and energy exchange during charge trapping of DNA [50] and in the pump-probe spectroscopic observation of discrete breathers [49]. QHD descriptions of thermal equilibrium and system-bath interactions were considered in Refs. [51] and [30,52], respectively. Thermal averaging can help to smooth out chaotic behavior in the transient region. The ability to reproduce the quantum effects seen with discrete breathers using an efficient semiclassical technique presents a significant step toward reducing the gap between simple models of quantum breathers and large, complex systems exhibiting the breather phenomenon.

## ACKNOWLEDGMENTS

The authors are grateful to Dr. Yuriy Pereverzev and Dr. Panagiotis Maniadis for fruitful discussions and comments on the manuscript. The research was funded by NSF Grant No. CHE-1050405.

[1] A. A. Ovchinnikov, Zh. Eksp. Teor. Fiz. **57**, 263 (1969) [Sov. Phys. JETP **30**, 147 (1970)].
[2] S. Aubry, Phys. D (Amsterdam, Neth.) **103**, 201 (1997).
[3] R. Scharf, Y. S. Kivshar, A. Sánchez, and A. R. Bishop, Phys. Rev. A **45**, R5369 (1992).
[4] D. K. Campbell, S. Flach, and Y. S. Kivshar, Phys. Today **57** (1), 43 (2004).
[5] S. Flach and A. V. Gorbach, Phys. Rep. **467**, 1 (2008).
[6] O. Bohigas, S. Tomsovic, and D. Ullmo, Phys. Rep. **223**, 43 (1993).
[7] P. Binder, D. Abraimov, A. V. Ustinov, S. Flach, and Y. Zolotaryuk, Phys. Rev. Lett. **84**, 745 (2000).
[8] B. Eiermann, T. Anker, M. Albiez, M. Taglieber, P. Treutlein, K.-P. Marzlin, and M. K. Oberthaler, Phys. Rev. Lett. **92**, 230401 (2004).
[9] B. I. Swanson, J. A. Brozik, S. P. Love, G. F. Strouse, A. P. Shreve, A. R. Bishop, W.-Z. Wang, and M. I. Salkola, Phys. Rev. Lett. **82**, 3288 (1999).
[10] G. T. Adamashvili, C. Weber, A. Knorr, and N. T. Adamashvili, Phys. Rev. A **75**, 063808 (2007).
[11] S. Pnevmatikos, A. V. Savin, A. V. Zolotaryuk, Y. S. Kivshar, and M. J. Velgakis, Phys. Rev. A **43**, 5518 (1991).
[12] P. Maniadis, B. S. Alexandrov, A. R. Bishop, and K. O. Rasmussen, Phys. Rev. E **83**, 011904 (2011).
[13] G. Kopidakis and S. Aubry, Phys. B (Amsterdam, Neth.) **296**, 237 (2001).
[14] A. V. Savin and Y. S. Kivshar, Europhys. Lett. **82**, 66002 (2008).
[15] S. Aubry, S. Flach, K. Kladko, and E. Olbrich, Phys. Rev. Lett. **76**, 1607 (1996).
[16] G. Kalosakas, A. R. Bishop, and V. M. Kenkre, J. Phys. B **36**, 3233 (2003).
[17] R. A. Pinto and S. Flach, Phys. Rev. A **73**, 022717 (2006).
[18] S. Flach and V. Fleurov, J. Phys.: Condens. Matter **9**, 7039 (1997).
[19] L. S. Schulman, D. Tolkunov, and E. Mihokova, Phys. Rev. Lett. **96**, 065501 (2006).
[20] L. Schulman, D. Tolkunov, and E. Mihkov, Chem. Phys. **322**, 55 (2006).
[21] J. Eilbeck and F. Palmero, Phys. Lett. A **331**, 201 (2004).
[22] O. V. Prezhdo and Y. V. Pereverzev, J. Chem. Phys. **116**, 4450 (2002).
[23] A. Pereverzev, Y. V. Pereverzev, and O. V. Prezhdo, J. Chem. Phys. **128**, 134107 (2008).
[24] E. M. Heatwole and O. V. Prezhdo, J. Chem. Phys. **130**, 244111 (2009).
[25] O. V. Prezhdo, J. Chem. Phys. **117**, 2995 (2002).
[26] O. Prezhdo, Theor. Chem. Acc. **116**, 206 (2006).
[27] D. S. Kilin, O. V. Prezhdo, and M. Schreiber, J. Phys. Chem. A **111**, 10212 (2007).
[28] H. Miyachi, Y. Shigeta, and K. Hirao, Chem. Phys. Lett. **432**, 585 (2006).
[29] A. Horsfield *et al.*, Comput. Mater. Sci. **44**, 16 (2008).
[30] K. Ando, Chem. Phys. Lett. **376**, 532 (2003).
[31] J. L. Gmez-Muoz, [http://homepage.cem.itesm.mx/lgomez/quantum/menuqhd.html].
[32] E. Pahl and O. V. Prezhdo, J. Chem. Phys. **116**, 8704 (2002).
[33] R. S. MacKay, Phys. A (Amsterdam, Neth.) **288**, 174 (2000).
[34] P. Maniadis, G. Kopidakis, and S. Aubry, Phys. D (Amsterdam, Neth.) **188**, 153 (2004).
[35] K. Igumenshchev, M. Ovchinnikov, and O. Prezhdo (unpublished).
[36] T. Dauxois and A. Litvak-Hinenzon, *Energy Localisation and Transfer*, Advanced Series in Nonlinear Dynamics (World Scientific, River Edge, NJ, 2004).
[37] E. J. Heller, J. Chem. Phys. **75**, 2923 (1981).
[38] M. F. Herman and E. Kluk, Chem. Phys. **91**, 27 (1984).
[39] K. G. Kay, Chem. Phys. **322**, 3 (2006).
[40] G. Hochman and K. G. Kay, J. Chem. Phys. **130**, 061104 (2009).
[41] D. V. Shalashilin, J. Chem. Phys. **132**, 244111 (2010).
[42] Y. Wu and V. S. Batista, J. Chem. Phys. **121**, 1676 (2004).
[43] Y. Wu and V. S. Batista, J. Chem. Phys. **118**, 6720 (2003).
[44] A. D. Ribeiro, M. A. M. de Aguiar, and M. Baranger, Phys. Rev. E **69**, 066204 (2004).
[45] W. H. Press, S. A. Teukolsky, W. T. Vetterling, and B. P. Flannery, *Numerical Recipes in C++: The Art of Scientific Computing*, 3rd ed. (Cambridge University Press, Cambridge, UK, 2002).
[46] E. J. Heller, J. Chem. Phys. **62**, 1544 (1975).
[47] M. Thoss, I. Kondov, and H. Wang, Phys. Rev. B **76**, 153313 (2007).
[48] M. Eleftheriou and S. Flach, Phys. D (Amsterdam, Neth.) **202**, 142 (2005).
[49] M. Ivanchenko, O. Kanakov, V. Shalfeev, and S. Flach, Phys. D (Amsterdam, Neth.) **198**, 120 (2004).
[50] G. Kalosakas, K. O. Rasmussen, and A. R. Bishop, J. Chem. Phys. **118**, 3731 (2003).
[51] E. M. Heatwole and O. V. Prezhdo, J. Chem. Phys. **126**, 204108 (2007).
[52] E. M. Heatwole and O. V. Prezhdo, J. Phys. Soc. Jpn. **77**, 044001 (2008).